Int. J. Electrochem. Sci., 5 **(2010)** 1972 - 1983

International Journal of
ELECTROCHEMICAL
SCIENCE
www.electrochemsci.org

Comparative Surface Electrochemistry of Co and Co_3O_4 Nanoparticles: Nitrite as an Analytical Probe

Abolanle S. Adekunle[1] *and Kenneth I. Ozoemena*[1,2,*]

[1] Department of Chemistry, University of Pretoria, South Africa.
[2] Energy and Processes Unit, Materials Science and Manufacturing, Council for Scientific and Industrial Research (CSIR), Pretoria 0001, South Africa.
[*]E-mail: kozoemena@csir.co.za

Received: 5 September 2010 / *Accepted:* 15 September 2010 / *Published:* 1 December 2010

This study described the decoration of edge plane pyrolytic graphite electrode (EPPGE) with synthesised cobalt and cobalt oxide nanoparticles. The modified electrode was characterised by techniques such as TEM, FESEM, XRD, EDS, cyclic voltammetry (CV) and electrochemical impedance spectroscopy (EIS). The EPPGE-Co demonstrated enhanced electron transport and catalytic efficiency towards nitrite oxidation at pH 7.4 compared with the other electrodes studied. The catalytic rate constant (*K*) obtained at the EPPGE-Co for nitrite at pH 7.4 is 2.32 x 10^6 $cm^3mol^{-1}s^{-1}$ while the limits of detection (LoD = 3.3 δ/m) is 7.3 x 10^{-7} M.

Keywords: Cobalt and cobalt oxide nanoparticles, electron transport, impedance spectroscopy, nitrite oxidation.

1. INTRODUCTION

Pure cobalt nanoparticles (2–20 nm) are of great research interest due to its unusual phenomena (quantum effects) and industrial applications [1,2]. They are used for magnetic, fluids, optoelectronics and in data storage [1-3]. On the other hand, cobalt oxide films are composed of nanosized metal oxide particles, and have been intensively investigated in recent years for their use in processes such as energy storage system [4], electrochromic thin films [5], magnetoresistive devices [6] and heterogeneous catalysis [7]. Electrodes modified with cobalt and its complexes have intensely been reported for the detection and sensing of several analytes [8-16] such as glucose [8,11], cysteine [9], hydrogen peroxide [10], hydroquinone [13], thiol-based nerve agents [14], epinephrine [15], and nitrite [16].

Nitrite ion is important as it is commonly used as an additive in some foods [17]. Other uses include color fixative and preservation in meats, manufacturing diazo dyes, in the textile industry, photography, manufacture of rubber chemicals, fertilizers in agriculture [18] and medicinal agents (used as a vasodilator [19]. It can be formed as a result of the degradation of some fertilizers and corrosion inhibitor [20]. Nitrite is one of the major components of waste water from nuclear power production [21] and can interact with amines to form carcinogenic nitrosamines [22]. Due to the importance of nitrite in the environmental sciences and in food chemistry, electrochemical detection of nitrite has been a subject of research and review [23].

Electrochemical technique may be preferred over other analytical probes due to its simplicity of fabrication, ease of miniaturisation, and low-cost.

Although there are many report on the synthesis of metal nanoparticles such as cobalt [24-28], it is surprising that most work focus more on electrocatalysis of theses metal nanoparticles other than their electron transport behaviour that form the basis for electrocatalysis. This study, for the first time, explores the surface electrochemistry of Co and Co_3O_4 nanoparticles as well as their electrocatalytic detection ability towards nitrite.

2.EXPERIMENTAL PART

2.1. Materials and Reagents

$Co(NO_3)_2.6H_2O$, $NaNO_2$ and other reagents were of analytical grade and used as supplied without further purification. Phosphate buffer solutions (PBS) at various pHs were prepared with appropriate amounts of $NaH_2PO_4.2H_2O$ and $Na_2HPO4.2H_2O$, and the pH adjusted with 0.1 M H_3PO_4 or NaOH. Ultra pure water of resistivity 18.2 MΩcm was obtained from a Milli-Q Water System (Millipore Corp., Bedford, MA, USA) and was used throughout for the preparation of solutions.

2.1.1. Syntheses of cobalt and cobalt oxide nanoparticles

Co nanoparticles were synthesized using the method described by Shen et al. [25]. 71.4 mg of $Co(NO_3)_2.6H_2O$ was dissolved in 20 mL ethylene-glycol / 5 mL H_2O. The precursor was reduced by slowly adding solution containing mixture of 0.1 M $NaBH_4$ and 1.0 M NaOH. The mixture was quickly heated to 120 ^oC for 2h to reduce the Co completely.

Cobalt oxide nanoparticles were prepared using the method described by Yao *et al*. [26]. Briefly, a known weight (3.0 g) of $Co(NO_3)_2.6H_2O$ was dissolved into 100 mL of isopropyl alcohol-water (1:1, v/v) solution in a three-necked round-bottom flask. Then appropriate amount of isopropyl alcohol-ammonia solution (45-50 mL) was added into the solution and aged for hours to ensure complete precipitation. The precipitate was filtered and dried under vacuum at 70 ^0C. The CO_3O_4 was finally obtained by calcining the $Co(OH)_2$ precursor at 500 ^0C in argon for 2h.

The resulting samples were investigated with high resolution scanning electron microscopy (HRSEM), transmission electron microscopy (TEM), and X-ray Diffractometry (XRD) using CoKα radiation.

2.2. Equipment and Procedure

The edge plane pyrolytic graphite (EPPG) plate was purchased from Le Carbone, Sussex, UK and was constructed locally by placing it in a teflon tube, extended outside with a copper wire to make electrical contact with the electrochemical equipment. Field emission scanning electron microscopy (FESEM) image was obtained using the Zeiss Ultra Plus 55 HRSEM (Germany).

Transmission electron microscopy (TEM) experiment was performed using a Model JEOL JEM-2100F field emission transmission electron microscope, Tokyo (Japan) while the XRD analysis was done using a back loading preparation method.

The sample was analysed using a PANalytical X'Pert Pro powder diffractometer (Netherland) with X'Celerator detector and variable divergence- and receiving slits with Fe filtered Co-Kα radiation.

Electrochemical experiments were carried out using an Autolab Potentiostat PGSTAT 302 (Eco-Chemie, Utrecht, The Netherlands) driven by the GPES software version 4.9. Electrochemical impedance spectroscopy (EIS) measurements were performed with an Autolab Frequency Response Analyser (FRA) software between 10 kHz and 10 mHz using a 5 mV rms sinusoidal modulation.

The FRA software allowed the fitting of the raw EIS data to equivalent circuit models using a *complex non-linear least squares* (CNLS) routine, with *Krammers-Kronig rule check*. A Ag|AgCl in saturated KCl and platinum wire were used as reference and counter electrodes, respectively. A bench top pH / ISE ORION meter, model 420A, was used for pH measurements. All solutions were de-aerated by bubbling nitrogen prior to each electrochemical experiment. All experiments were performed at 25±1 °C.

2.3. Electrode Modification and Pretreatments

EPPGE surface was cleaned by gentle polishing in aqueous slurry of alumina nanopowder (Sigma-Aldrich) on a SiC-emery paper and then to a mirror finish on a Buehler felt pad. The electrode was then subjected to ultrasonic vibration in absolute ethanol to remove residual alumina particles that might have been trapped at the surface.

EPPGE was modified by drop-dry method. Different weights (2.5 to 10 mg) of the synthesised Co and Co_3O_4 nanoaparticles were weighed and dissolved in 1 mL dimethylformamide (DMF).

The mixture was stirred at room temperature for 48 h. About 20 µL of the solution was drop-cast on the EPPGE and annealed in the oven at 50^0 C for 5 min. The modified electrode is denoted as EPPGE-Co or the EPPGE-Co_3O_4.

3. RESULTS AND DISCUSSION

3.1. Characterisation with TEM, HRSEM and XRD

Figure 1a and b showed the comparative transmission electron microscopy (TEM) images of Co (a) and the Co_3O_4 nanoparticles while (b) while Figure 1c and d are their corresponding FESEM images. The Co nanoparticles form amorphous nanoparticles (Fig. 1a and 1c). On the other hand, Co_3O_4 nanoparticles appeared crystalline (Fig. 1b). The crystals aggregated and form a web-like structure (Fig. 1d). From the TEM result, the size of most of the particles is in 20 to 50 nm for Co and 10 to 30 nm for the Co_3O_4.

The XRD spectra for the nanosized particles are shown in Fig. 2. The nanoscaled Co (Figure 2a) is characterised by XRD peaks at 2θ of 47.9^o, 59.8^o and 79.6^o which could be assigned to (111), (200) and (222) of a cubic structures Co nanoparticles [27,28]. The Co_3O_4 nanaoparticles (Fig. 2b) show characteristic peaks at 2θ of 22.1, 36.5, 43.1, 45.1, 52.5, 57.7, 65.7, 70.2 and 77.5 due to the indices of (111), (220), (311), (222), (400), (331), (422), (511) and (440) corresponding to Cubic Fd-3m Co_3O_4 crystal lattice [28,29]. From Debye-Scherrer equation [30,31], average crystalite size of 22.8 nm was obtained which is in consistent with the TEM result.

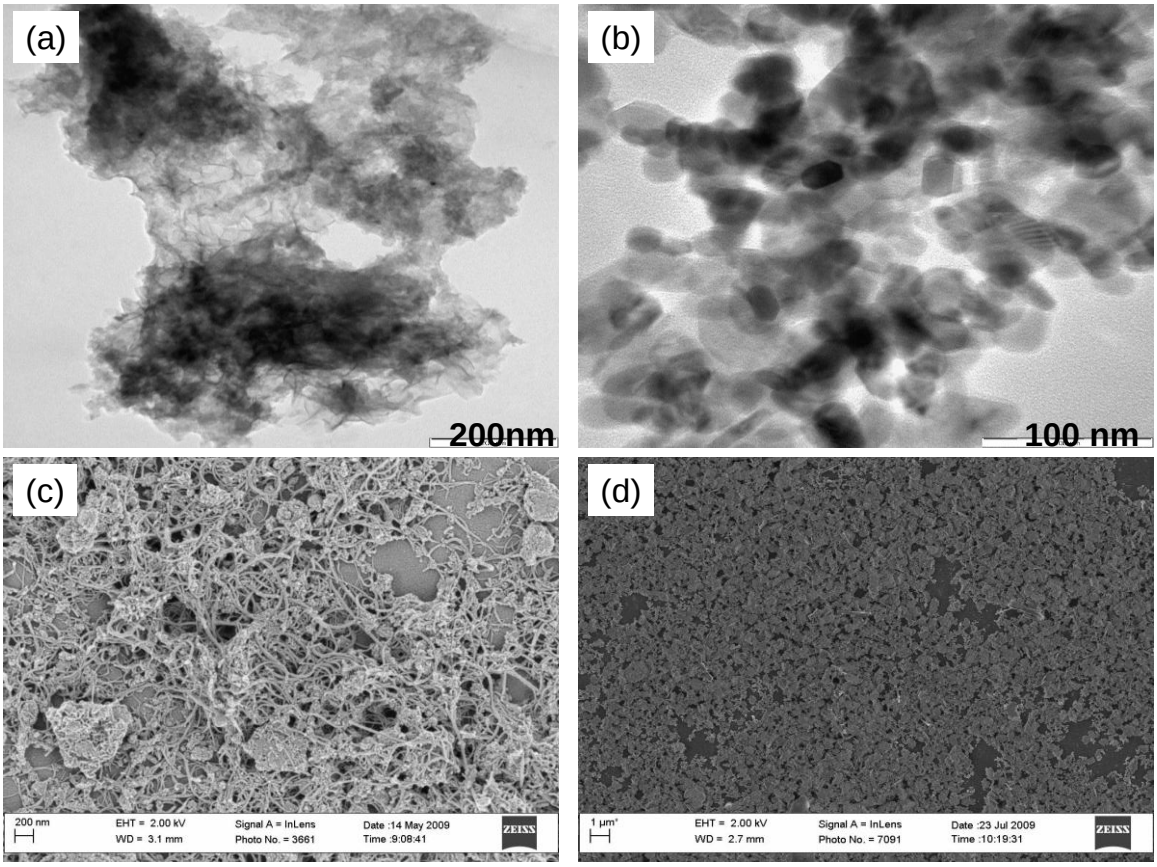

Figure 1. TEM images of (a) Co and (b) Co_3O_4 nanoparticles. Figure 1c and d are the FESEM micrographs of Co and Co_3O_4 nanoparticles, respectively.

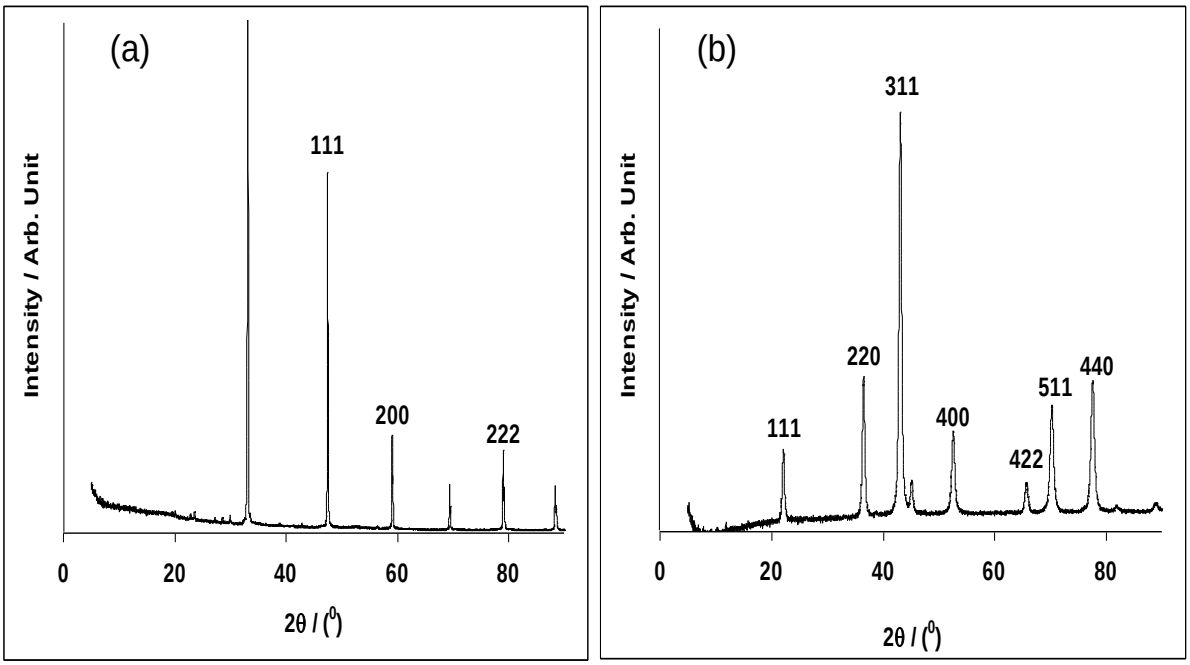

Figure 2. XRD spectra of Co (a) and Co_3O_4 (b) nanoparticles.

3.2. Comparative Electrochemical characterization

Figure 3 compares the current response of the bare and the modified electrodes in (a) 0.1 M PBS (pH 7.0) and (b) 5 mM $Fe(CN)_6]^{4-}/[Fe(CN)_6]^{3-}$ solution. In Figure 3a, the electrode based on the Co nanoparticles showed broad anodic peak at *ca* 0.6 V, presumable due to the formation of Co_3O_4 through the reaction:

$$3Co(OH)_2 + 2OH^- \longrightarrow Co_3O_4 + 4H_2O + 2e^- \qquad (1)$$

The broadness of the peak may be due to the formation of other oxidation products as represented by the equation below [32]:

$$Co(OH)_2 + OH^- \longrightarrow CoOOH + H_2O + e^- \qquad (2)$$

The cathodic peaks observed at ca 0.52 and 0.22 V are attributed to the reduction of CoOOH to $Co(OH)_2$ or Co_3O_4. Interestingly, the electrodes based on the Co_3O_4 nanoparticles did not show recognisable redox process as the Co nanoparticles in the neutral pH conditions used.

Next, we questioned the extent to which these electrodes mediate the electron transport of the redox probe, $Fe(CN)_6]^{4-}/[Fe(CN)_6]^{3-}$, to and from the underlying electrodes. Two redox couples are noticed for the electrodes in $Fe(CN)_6]^{4-}/[Fe(CN)_6]^{3-}$ solution (Fig. 3b); the redox couples in the 0 – 0.3 V region being attributed to the $Fe(CN)_6]^{4-}/[Fe(CN)_6]^{3-}$ redox process, while the redox couples in the

0.3 – 0.7 V region correspond to cobalt processes. Electrochemical impedance spectroscopy (EIS) experiment was carried at fixed potential of 0.2 V (the equilibrium potential, $E_{1/2}$, of the $[Fe(CN)_6]^{4-}$ /$[Fe(CN)_6]^{3-}$ couple). The Nyquist plot obtained (Fig. 4) was satisfactorily fitted using the modified Randles electrical equivalent circuit model shown in the inset.

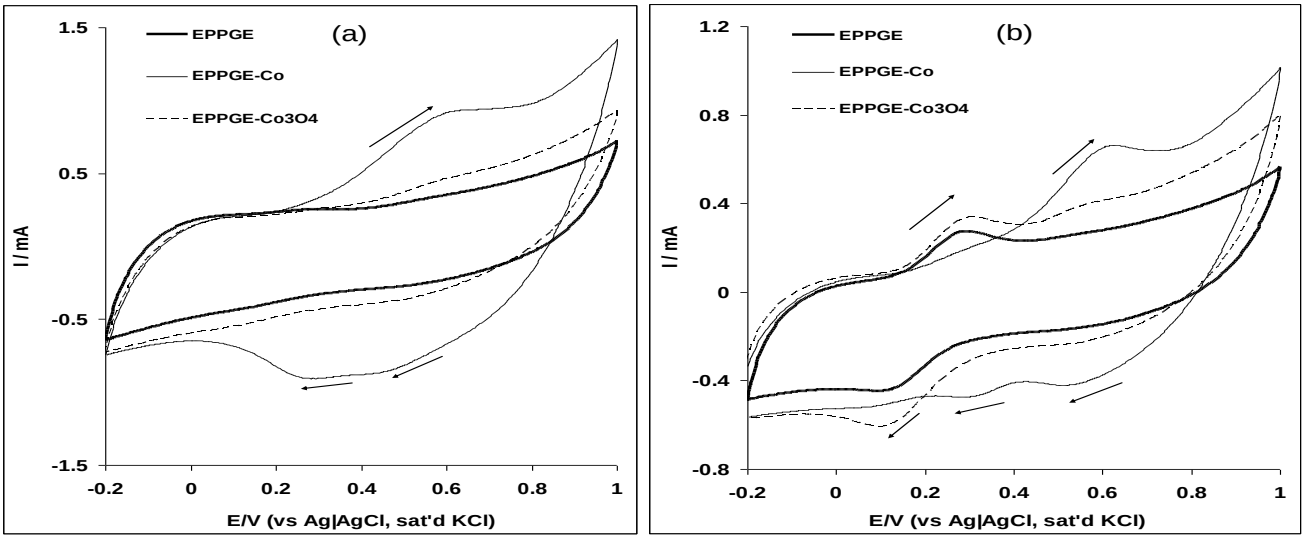

Figure 3. Comparative cyclic voltammetric evolutions of the EPPGE, EPPGE-Co and EPPGE-Co_3O_4 electrodes in (a) 0.1 M PBS (scan rate = 100 mVs^{-1}), and (b) 5 mM $[Fe(CN)_6]^{4-}$/$[Fe(CN)_6]^{3-}$ solution in pH 7.0 PBS (scan rate = 50 mVs^{-1}).

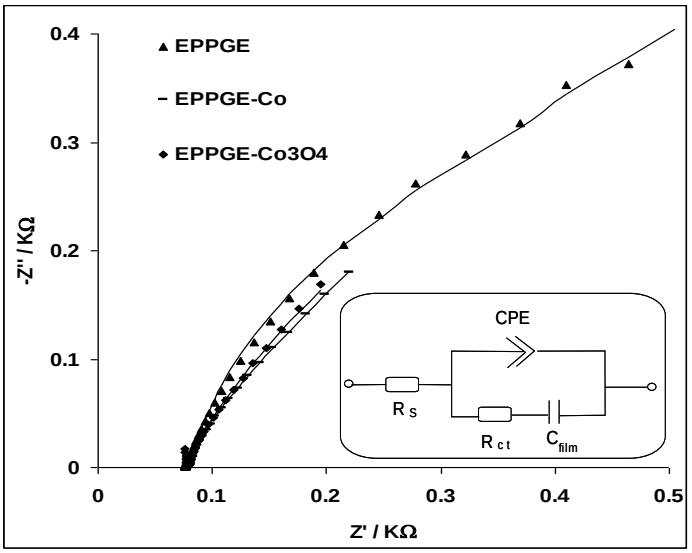

Figure 4. Typical Nyquist plots obtained for the electrodes in 5 mM $[Fe(CN)_6]^{4-}$ / $[Fe(CN)_6]^{3-}$ solution at a fixed potential of 0.2 V (vs Ag|AgCl, sat'd KCl). The data points are experimental while the solid lines in the spectra represent non-linear squares fits. Inset in Figure 4 is the circuit used in the fitting of the EIS data.

In this model, the constant phase element CPE described the porous nature of the electrode, R_s is the solution/electrolyte resistance, R_{ct} represents the charge-transfer resistance and C_{film} describes the high pseudocapacitive nature of the system. The R_{ct} values follow the trend: EPPGE-Co (0.36 Ωcm^2) < EPPGE-Co_3O_4 (0.60 Ωcm^2) << bare-EPPGE. The modified electrodes showed lower R_{ct} values compared to the bare EPPGE, indicating that the nanoparticle catalysts enhance electron transfer of the redox probe compared to the unmodified EPPGE.

Table 1. Impedance data obtained for EPPGE, EPPGE-Co and EPPGE-Co_3O_4 electrodes in 5 mM $Fe(CN)_6]^{4-}/[Fe(CN)_6]^{3-}$ solution at 0.2 V (vs Ag|AgCl sat'd KCl). All values were obtained from the fitted impedance spectra after several iterations using the circuits.

Electrode	Impedimetric Parameters				
	R_s / Ωcm^2	CPE / μFcm^{-2}	n	R_{ct} /Ωcm^2	C_{film} / $mFcm^{-2}$
EPPGE	7.02±0.01	0.82±0.35	0.40±0.01	1.23±0.02	3.09±0.11
EPPGE-Co	7.80±0.01	216.40±25.47	0.50±0.01	0.36±0.01	13.02±0.34
EPPGE-Co_3O_4	7.57±0.01	381.3±13.01	0.52±0.05	0.60±0.04	15.98±3.77

3.3. Comparative electrocatalysis towards nitrite

Comparative current responses of the electrodes in 10^{-3} M NO_2^- (in pH 7.4 PBS) are presented in Figure 5.

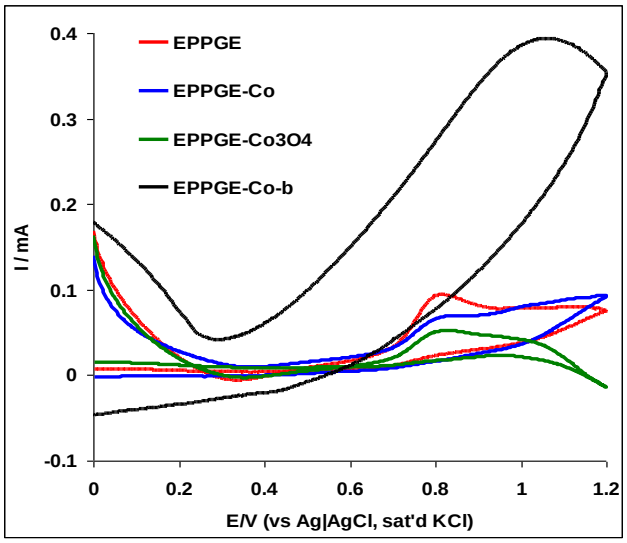

Figure 5. Comparative current response of (a) EPPGE, EPPGE-Co and EPPGE-Co_3O_4 (after background current subtraction) in pH 7.4 PBS containing 1.0 mM NO_2^- solution (scan rate = 25 mVs^{-1}). EPPGE-Co-b represents 7.5 mg mL^{-1} Co loading in pH 7.4 PBS containing 1.0 mM NO_2^- solution.

At 2.5 mg mL^{-1} Co loading, the current responses in NO_2^- follow the order: bare EPPGE (43.7 µA) > EPPGE-CoO (21.0 µA) > EPPGE-Co (18.0 µA) (Fig. 5). The result agreed with the recent report by Compton group [33] in terms of onset potential of catalysis and the peak potential for nitrite oxidation on bare glassy carbon electrode. However, at 7.5 mg mL^{-1} Co and Co_3O_4 loading, EPPGE-Co gave the highest current response (83.0 µA) with lower onset potential (0.3 V) of catalysis which is ~ 380 mV lower than *ca* 0.67 V recorded for the other electrodes (Fig. 5). At this loading, its current response was ~ 2 times the bare EPPGE and 2.5 times EPPGE-CoO. Thus, contribution of modified electrode to reducing nitrite overpotential on bare electrode, and in enhancing its oxidation current are a possibility, which may depend on the method of modification, the nature of the electrocatalyst and amount used in modifying the electrode. The present results also show enhanced electrochemical performance compared to several reports, including the recent work incorporating carbon nanotubes [34] in terms of onset potentials and current response. To our surprise, our attempts to use CNTs as supports for these synthesised Co and Co_3O_4 nanoparticles did not improve the electrochemistry of nitrite, a further advantage of these metal nanoparticles over their electrodeposited counterparts that require CNTs. Since EPPGE-Co electrode proved to be better towards nitrite oxidation, all further studies were carried out with it, unless otherwise stated.

The catalytic behaviour of the electrodes towards nitrite oxidation was also investigated using EIS. The Nyquist plots obtained for the electrodes during nitrite oxidation at pH 7.4 (at fixed potential of 0.8 V vs Ag|AgCl, sat'd KCl) is presented in Figure 6. A modified Randles circuit model already discussed above (inset in Fig. 4) satisfactorily fitted the data from nitrite oxidation (Table 2). The C_{film} is replaced by C_{ads} which is attributed to the high capacitive nature of the synthesised Co and CoO nanopartilces or adsorption of NO_2^- intermediate product on the electrode. The low R_{ct} of the EPPGE-Co (0.31 Ωcm^2) compared with the bare EPPGE (0.36 Ωcm^2) and EPPGE-Co_3O_4 (0.46 Ωcm^2) also explain the good electron transport and catalysis witness at the electrode.

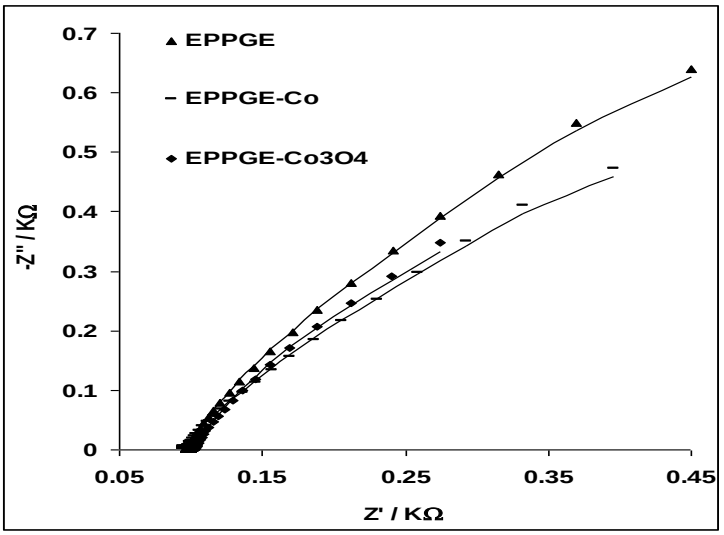

Figure 6. Typical Nyquist plots obtained for EPPGE, EPPGE-Co and EPPGE-Co_3O_4 in 1.0 mM NO_2^- solution at a fixed potential of 0.8 V (vs Ag|AgCl, sat'd KCl). The data points are experimental while the solid lines in the spectra represent non-linear squares fits.

Table 2: Impedance data obtained for some of the electrodes in 1.0 mM NO_2^- (in PBS pH 7.4 at 0.80 V vs Ag|AgCl sat'd KCl. All values were obtained from the fitted impedance spectra after several iterations using the circuit.

Electrode	Impedimetric Parameters				
	R_s / Ωcm^2	CPE / μFcm^{-2}	n	R_{ct} / Ωcm^2	C_{ads} /$mFcm^{-2}$
EPPGE	9.48 ±0.01	133.8±35.39	0.59±0.01	0.36±0.01	6.98±0.30
EPPGE-Co	9.31±0.01	170.6±48.80	0.57±0.01	0.31±0.01	6.83±0.43
EPPGE-Co_3O_4	10.00±0.01	160.4±42.17	0.55±0.02	0.46±0.01	17.07±0.87

Cyclic voltammograms showing the current responses in NO_2^- with increasing scan rates were also studied (25 – 500 mVs^{-1}). A shift in potential with increase in scan rate was observed. The plot of the peak current (I_p) against the square root of scan rate ($\nu^{1/2}$) gave a linear relationship (R^2 = 0.9915) with a positive intercept, suggesting a diffusion-controlled process.

For a totally irreversible, diffusion-controlled process, the following relationship holds [35]:

$$Ep = \frac{b}{2}\log \nu + const. \qquad (3)$$

$$b = \frac{2.303RT}{\alpha n_\alpha F} \qquad (4)$$

where *R*, *T* and *F* have their usual meaning, *b* is the Tafel slope, n is the number of electrons involved in the rate-determining step, and α is the electron transfer coefficient. There was a linear relationship between the peak potential E_p and the logν(not shown), which confirms the chemical irreversibility of nitrite electrocatalytic oxidation process. The value of the Tafel slope is somewhat huge (540.8 mV dec^{-1}) compared to the normal reported values for various analytes including nitrite [34], although such high values (up to 650 $mVdec^{-1}$) have also been observed by others [36]. High Tafel values generally indicate binding of the analyte or its intermediates on the electrode surface, or reactions occurring within a porous electrode structure [37].

From the above discussion, the electrocatalytic response of NO_2^- at EPPGE-Co may be represented as proposed for cobalt complex [38]:

$$[Co]_{film} + H_2O \longrightarrow [Co^{2+}]_{film\ (aq)} + e^- \quad (5)$$

$$[Co^{2+}]_{film} + NO_2^- \rightleftharpoons [Co^{2+}\text{---}(NO_2^-)]_{adduct} \quad (6)$$

$$[Co^{2+}\text{---}(NO_2^-)]_{adduct} \rightleftharpoons [Co^{3+}]_{film} + NO_2 + e^- \ (slow) \quad (7)$$

$$2NO_2 + H_2O \rightleftharpoons 2H^+ + NO_3^- + NO_2^- \quad (8)$$

$$NO_2^- + H_2O \longrightarrow 2H^+ + NO_3^- + 2e^- \quad (9)$$

$$[Co^{3+}] + e^- \longrightarrow [Co^{2+}]_{film} \quad (10)$$

The nitrite ion interact with the Co(II) film forming an adduct (Eqn. 6). This step represents the adsorption process. Equation 7 is assumed to be the rate-determining step which is a one-electron process. The oxidation of the Co(II) to Co(III) simultaneously leads to the generation of the nitrogen dioxide. The formation of the NO_2 (Eqn. 7) is followed by its disproportionation to give nitrite and nitrate (Eqns. 8 and 9). Co(III) is reduced to regenerate the Co(II) (Equation 10).

Next, we studied the effect of current response on varying concentrations of nitrite using chronamperometric technique (Figure 7). Plot of current response versus nitrite concentration (inset in Fig.7) gave a linear relationship (Y = (1.32±0.01)X + 16.82±0.29 (R^2 = 0.9996)) and sensitivity of 1.32±0.01 µA μM^{-1}. The limit of detection (LoD = 3.3 δ/m [39], where δ is the relative standard deviation of the intercept and *m*, the slope of the linear current versus the concentration of NO_2^-) was calculated as 0.73 µM. The 0.73 µM detection limit obtained is about 8 times lower than reported for the SWCNT-Co [34].

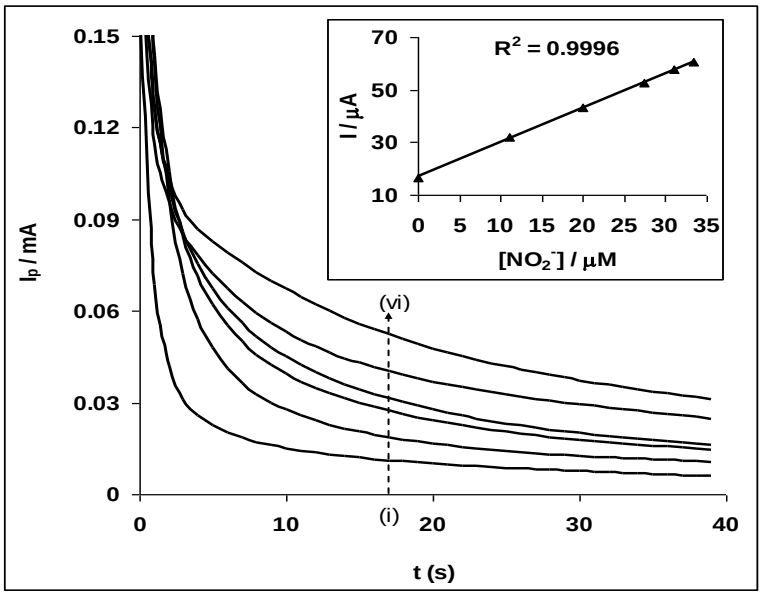

Figure 7: Typical chronoamperogram of EPPGE-Co in (a) 0.1 M PBS pH 7.4 containing different concentration of NO_2^- (0.0, 11.1, 20.0, 27.3, 31.0 and 33.3 µM (i to vi)). Inset is the plot of peak current (I_p) versus NO_2^- concentrations.

Nitrite at neutral pH has been detected at 4.0 µM using thionin/multiwalled carbon nanotubes/glassy carbon modified electrode [40] and myoglobin/ZnO/graphite modified electrode [41], 1.2 µM on haemoglobin/colloidal gold nanoparticles/TiO_2-sol gel film/GCE modified electrode [42],

Using Equation 11 [43,44]:

$$\frac{I_{cat}}{I_L} = \pi^{1/2}(kC_o t)^{1/2} \qquad (11)$$

where I_{cat} and I_l are the currents in the presence and absence of nitrite, k is the catalytic rate constant, C_o is the bulk concentration and t is the elapsed time. From the plot of I_{cat}/I_l vs $t^{1/2}$ (not shown) the catalytic rate constant for nitrite was obtained as 2.32 x 10^6 cm^3 $mol^{-1}s^{-1}$. This result is close to the 6.03 x 10^6 M^{-1} s^{-1} reported for the electrocatalytic reduction of nitrite at Vanadium–Schiff base complex/MWCNTs modified GC electrode [45].

4. CONCLUSIONS

Electrocatalytic detection of nitrite at edge-plane pyrolytic graphite electrodes (EPPGEs) modified Co/ Co_3O_4 was studied. The cyclic voltammetry and EIS studies showed that the EPPGE-Co have better current response and low charge transfer resistance compared with EPPGE-Co_3O_4 and the bare EPPGE in $[Fe(CN)_6]^{4-/3-}$ redox probe. However, EPPGE-Co gave best catalysis towards nitrite oxidation especially at higher Co loading in pH 7.4. The electrode followed an adsorption controlled electrode process judge by its high Tafel values of 540.8 for NO_2^-. The limit of detection and the catalytic rate constant of the electrode in the analytes agreed favourably with values reported earlier in literature.

ACKNOWLEDGEMENTS
We thank the National Research Foundation (NRF) for their support. ASA thanks NRF and the University of Pretoria for graduate bursaries and Obafemi Awolowo University Ile-Ife, Nigeria, for a PhD study leave.

References

1. H. Gleiter, *Prog Mater Sci*, 33 (1989) 223.
2. J.P. Chen, C.M. Sorensen, K.J. Klabunde, G.C. Hadjipanayis, *Phys Rev B*, 51 (1995) 11527.
3. K. Tanabe, *Mater. Lett.*, 61 (2007) 4573.
4. V. Srinivasan, J.W. Weidner, *J. Power Sources*, 108 (2002) 15.
5. L.D. Kadam, S.H. Pawar, P.S. Patil, *Mater. Chem. Phys.*, 68 (2001) 280.
6. H. Okabe, J. Akimitsu, T. Kubodera, M. Matoba, T. Kyomen, M. Itoh, *Phys. B Condens. Matter.* 378 (2006) 863.

7. A. Salimi, R. Hallaj, H. Mamkhezri, S. Mohamad, T. Hosaini, *J. Electroanal. Chem.*, 619-620 (2008) 31.
8. I.G. Casella, M.R. Guascito, *J. Electroanal. Chem.*, 476 (1999) 54.
9. I.G. Casella, M. Gatta, *J. Electroanal. Chem.*, 534 (2002) 31.
10. K.I. Ozoemena, Z.X. Zhao, T.Nyokong, *Electrochem. Commun.*, 7 (2005) 679.
11. K.I. Ozoemena, T. Nyokong, *Electrochim. Acta*, 51(2006) 5131.
12. K.I. Ozoemena, J. Pillay, T. Nyokong, *Electrochem. Commun.*, 8 (2006) 1391.
13. L.F. Fan, X.Q. Wu, M.D. Guo, Y.T. Gao, *Electrochim. Acta*, 52 (2007) 3654.
14. J. Pillay, K.I. Ozoemena, *Electrochim. Acta*, 52 (2007) 3630.
15. K.I. Ozoemena, D. Nkosi, J. Pillay, *Electrochim. Acta* 53 (2008) 2844.
16. A. Salimi, H. Mamkhezri, R. Hallaj, S. Soltanian, *Sens. Actuat. B*, 129 (2008) 246.
17. C.A. Caro, F. Bedioui, J.H. Zagal, *Electrochim. Acta*, 47 (2002) 1489.
18. N.S. Bryan, *Free Radical Biol. Med.*, 41 (2006) 691.
19. E.T. Reichert, S.W. Mitchell, *Am. J. Med. Sci.*, 159 (1980) 158.
20. H.J. Choi, G. Kwag, S. Kim, *J. Electroanal. Chem.*, 508 (2001) 105.
21. N. Sparatu, T.N. Rao, D.A. Tryk, A. Fujishima, *J. Electrochem. Soc.*, 148 (2001) E112.
22. Z.H. Wen, T.F. Kang, *Talanta*, 62 (2004) 351.
23. M.J. Moorcroft, J. Davis, R.G. Compton, *Talanta*, 54 (2001) 785
24. H. Karami, E. Mohammadzadeh, *Int. J. Electrochem. Sci.*, 5 (2010) 1032.
25. J. Shen, Y. Hu, C. Li, C. Qin, M. Ye, *Electrochim. Acta*, 53 (2008) 7276.
26. W-L. Yao, J-L. Wang, J. Yang, G-D. Du, *J. Power Sources*, 176 (2008) 369.
27. H. Shao, Y. Huang, H. Lee, Y.J. Suh, C.O. Kim, *Current Applied Physics*, 6S1 (2006) e195.
28. M. Hamdani, R.N. Singh, P. Chartier, *Int. J. Electrochem. Sci*., 5 (2010) 556.
29. M. Salavati-Niasari, F. Davar, M. Mazaheri, M. Shaterian *J. Magnetism Magnetic Materials*, 320 (2008) 575.
30. Y-K. Sun, M. Ma, Y. Zhang, N. Gu, Coll. Surf. A: *Physicochem Eng Aspects*, 245 (2004) 15.
31. R.M. Cornell, U. Schertmann, Iron Oxides in the laboratory: Preparation and Characterization, VCH, Weinheim (1991).
32. A. Salimi, R. Hallaj, S. Soltanian, H. Mamkhezri, *Anal. Chim. Acta*, 594 (2007) 24.
33. B.R. Kozub, N.V. Rees, R.G. Compton, *Sens. Actuat*. B 143 (2010) 539.
34. A.S. Adekunle, J. Pillay, K.I. Ozoemena, *Electrochim. Acta*, 55 (2010) 4319.
35. J.A. Harrison, Z.A. Khan, *J. Electroanal. Chem.*, 28 (1970) 131-138.
36. W. Chen, D. Ny, S. Chen, *J. Power Sources*, 195 (2010) 412.
37. J.N. Soderberg, A.C. Co, A.H.C. Sirk, V.I. Birss, *J. Phys. Chem. B*, 110 (2006) 10401.
38. F. Armijo, M.C. Goya, M. Reina, M.J. Canales, Arevalo MC, M.J. Aguire *J. Mol. Cat.* A, (2007) 268.
39. G.D. Christian, *Analytical Chemistry*, 6th ed., John Wiley and Sons, New York p. 113 (2004).
40. A. Salimi, A. Noorbakhash, F.S. Karonian, *Int. J. Electrochem. Sci.*, 1 (2006) 435.
41. G. Zhao, J.J. Xu, H.Y. Chen, *Anal. Biochem.* 350 (2006) 145.
42. W. Yang, Y. Bai, Y. Li, C. Sun, *Anal. Bioanal. Chem.*, 382 (2005) 44.
43. P. Santosh, K.M. Manesh, A.I. Gopalan, K.P. Lee, *Electroanalysis*, 18 (2006) 894.
44. Z. Galus, *Fundamentals of Electrochemical Analysis*, Ellis Horwood Press, New York, 1976, p. 313, Ch. 10
45. A. Salimi, H. Mamkhezri, S. Mohebbi, *Electrochem. Commun.*, 8 (2006) 688.